

In vitro anticancer and antitubercular activities of cellulose-magnetite nanocomposite synthesized using deep eutectic solvent as a dispersant

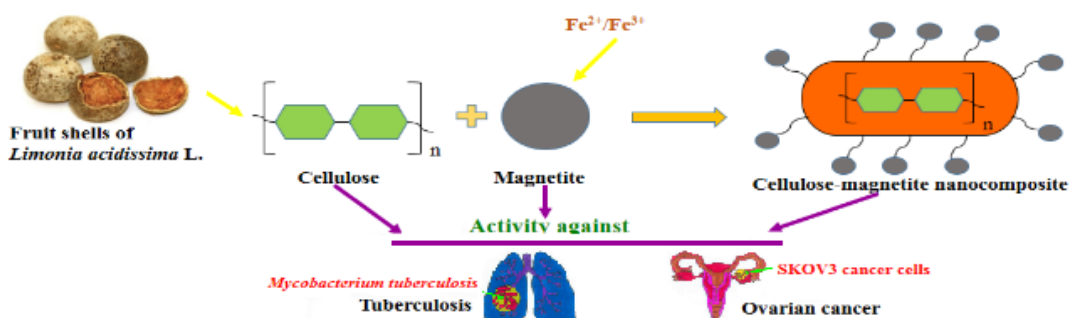
Swathi Pon Sakthi Sri. V, Mary George*

Department of Chemistry, Stella Maris College (Autonomous), University of Madras, 17, Cathedral Road, Chennai, Tamil Nadu – 600 086, India.

Submitted on: 08-Jan-2021, Accepted and Published on: 7-Feb-2021

ABSTRACT

In the current scenario, Deep Eutectic Solvents (DESs) are persuasive greener solvents for the successful synthesis of different nanostructures due to their tunable properties with enhanced applications. We report here the successful formation of a nanocomposite based on cellulose and magnetite nanoparticles.



The method of isolating cellulose from fruit shells of *Limonia acidissima* (L.) as detailed in the work is described for the first time. Magnetite nanoparticles were synthesized through the cost effective co-precipitation method and DES embracing choline chloride and fructose were used as non-toxic dispersant for the synthesis of cellulose-magnetite nanocomposite. Various physiochemical parameters like compositional, structural, morphological and magnetic properties are analyzed using FTIR, XRD, HRTEM, SAED and VSM techniques. Anticancer and antitubercular activities, performed by MTT and LRP assays respectively, reveals that the IC₅₀ values for cellulose, magnetite and cellulose-magnetite nanocomposite are found to be 20.65 µg/ml, 44.66 µg/ml and 8.685 µg/ml and cellulose-magnetite nanocomposite shows 51.95% inhibition at 200 µg/ml concentration against *Mycobacterium tuberculosis*. The obtained results suggest that the prepared cellulose-magnetite nanocomposite can serve as a potential candidate for drug designing with the use of green solvents.

Keywords: Ovarian carcinoma, Tuberculosis, *Limonia acidissima* (L.), Deep eutectic solvents (DESs), Nanocomposite

INTRODUCTION

The World Health Organization (WHO) warns that within the next two decades, the world will see a 60% rise in cancer cases.¹ Cancer commonly describes many diseases that are characterised by unregulated cell proliferation triggered by the disruption or dysfunction of regulatory signaling pathways.² One of the main causes of disease and death linked to

carcinomas affecting women globally is ovarian carcinoma.³ Ovarian carcinomas emerge mainly from nodules of the ovarian surface epithelium or postovulatory inclusion formed after follicular rupture and repair.⁴ Thus, the discovery and quest for novel and efficient anticancer agents is very significant.⁵ Moreover, the new WHO study reports that about a quarter of the world's population is infected with *Mycobacterium tuberculosis* and thus at risk of contracting tuberculosis disease.⁶ Tuberculosis (TB), caused by a bacterium called *M. tuberculosis*, is the second deadliest infectious disease next to Acquired Immune Deficiency Syndrome (AIDS). *Mycobacterium* affects the lungs primarily, although other parts of the body, such as the kidney, lymphatic system, central nervous system, circulatory system, genitourinary system, bones, and joints, can also be affected. In this regard, the drug delivery system based on nanotechnology has many advantages,

*Corresponding Author: Dr. Mary George, Associate Professor, Department of Chemistry, Stella Maris College (Autonomous), Affiliated to University of Madras, 17, Cathedral Road, Chennai, Tamil Nadu – 600 086, India. Tel: +91 9092832700

Email: maryge@gmail.com marygeorge@stellamariscollege.edu.in

Cite as: J. Mater. NanoSci., 2021, 8(1), 1-10.

URN:NBN:sciencein.jmns.2021.v8.137

© ScienceIn Publishing ISSN: 2394-0867 <http://thesciencein.org/jmns>

such as nominal side effects compared to traditional drugs, high carrier power, precise drug release, and enriched tuberculosis treatment compliance.⁷

Limonia acidissima (L.), known locally as the wood apple, belongs to the monotypic genus *Limonia* Rutaceae family, confined to India, Pakistan, Sri Lanka and Southeast Asia. There have been several reports on the biomedical applications of various sections of *Limonia acidissima* (L.) such as leaves, fruit pulp, and bark including antibacterial, antidiabetic, antifungal, wound healing, anticancer, antidiarrheal, antihistamine activities, etc.⁸ The surplus fruit shell of *Limonia acidissima* (L.) has been used as a biosorbent for the degradation of organic pollutants.^{9,10} Cellulose in the form of nanorods with an average length of 250-480 nm and diameter 20-60 is produced from sugarcane bagasse.¹¹ Isolation of cellulose nanofibers from banana peels is achieved using (*Musa sapientum* L.).¹² Cellulose is extracted from kapok banana peel (*Musa parasidiaca* L.) and the product is used for the removal of procion dye.¹³ Cellulose is isolated from different fruit and vegetable pomaces such as *Malus domestica* Borkh, *Solanum lycopersicum* (L.), *Cucumis* (L.) and *Daucus carota* (L.).¹⁴ Recently, cellulose nanofibers are produced from banana peel by chemical and mechanical treatments, further cytotoxicity is further assessed against human colon carcinoma Caco-2 cells.¹⁵ An environmentally friendly synthesis process has been reported with the aid of *Syzygium aqueum* (water apple) leaves extract for the preparation of supported PdNPs for the conversion of Suzuki-Miyaura coupling products.^{16,17}

However there is no substantiation for the isolation of cellulose from the fruit shells of *Limonia acidissima* (L.). Magnetic nanomaterials based on cellulose have immense uses as magnetic resonance imaging, adsorbents and as eco-friendly catalysts¹⁸ reinforcing the reliability of the work.

Deep eutectic solvents (DESs) are typically formed by combining two or more components with a slightly lower melting point compared to their components.^{19,20} They have tremendous industrial applications due to their incredible properties such as humidity resistance, negligible vapour pressure, non-flammability, high thermal stability, less expensive, non-toxicity, reusability and environmentally benignity.²¹ During their synthesis reaction, DESs can effectively disperse nanoparticles.²² Among the various hydrogen bond acceptors that are available, choline chloride manifests remarkable importance as it is a recognised component of vitamin B²³ and serves as a major public health dietary source.²⁴ As fructose is an essential medicinal product among the list the hydrogen bond donors,²⁵ we intend to use the combination of choline chloride and D-Fructose for the deep eutectic solvent formation (DES). We hypothesize that biological activities can be enhanced by using these natural components.

In this work, we present the synthesis of cellulose-magnetite nanocomposite using ChCl:D-Fructose based DES. The individual counterparts of the composite is prepared by the isolation of cellulose from fruit shells of *Limonia acidissima* (L.) and by the synthesis of magnetite nanoparticles by co-

precipitation method. The compositional, structural, and magnetic analysis of the nanocomposite have been investigated using Fourier Transform infrared spectroscopy (FTIR), X-ray diffraction (XRD), Transmission electron microscopy (TEM), Selected area electron diffraction (SAED) and Vibrational sample magnetometry (VSM) techniques respectively. Also, the characterized nanomaterials are tested to study their effect on SKOV3 human ovarian carcinoma cells and *Mycobacterium tuberculosis* H37Rv pathogen for their use in the treatment of cancer and tuberculosis.

MATERIALS AND METHODS

Chemicals used

Iron dichloride tetrahydrate ($\text{FeCl}_2 \cdot 4\text{H}_2\text{O}$) was purchased from Sigma-Aldrich. Iron trichloride hexahydrate ($\text{FeCl}_3 \cdot 6\text{H}_2\text{O}$) was bought from Loba Chemie Pvt. Ltd. Mumbai, India. Urea ($\text{CO}(\text{NH}_2)_2$) and sodium hydroxide (NaOH) were obtained from Merck Life Science Pvt. Ltd. Mumbai, India. 30% hydrogen peroxide (H_2O_2) was purchased from NICE Chemicals Pvt. Ltd., Kerala, India. D-Fructose ($\text{C}_6\text{H}_{12}\text{O}_6$), choline chloride ($\text{C}_5\text{H}_{14}\text{ClNO}$), MTT (3-(4,5-dimethylthiazol-2-yl)-2,5-diphenyltetrazolium bromide), Dulbecco's Modified Eagle's medium (DMEM), dimethyl sulfoxide (DMSO), Fetal bovine serum (FBS), Streptomycin sulphate, Penicillin, glycerol, calcium chloride (CaCl_2), D-luciferin, G7H9 broth, albumin dextrose were procured from HiMedia Laboratories, Mumbai, India. The purity of these chemicals were more than 97 %. Solvents used in this protocol were of HPLC grade.

Sample collection, authentication and processing

Fruits of *Limonia acidissima* (L.) were collected from the campus of Stella Maris College (13°2'49" N 80°15'13" E), Chennai, Tamil Nadu, and India in September. The fresh samples were identified and authenticated with reference number PARC/2018/3818. The fruit shells were washed, shade dried, crushed using a pulveriser to acquire powder. The ground fruit shell powder was stored in an air-tight container in the refrigerator at 4°C for further usage.

Isolation of cellulose

100 g of *Limonia acidissima* (L.) fruit shell powder was treated with 600 mL hot distilled water for 10 minutes and filtered. The residue was treated with 600 mL of 1 M HCl at 85°C for 30 minutes and filtered. This step was repeated using 0.5 M HCl. The filtered residue was treated with 600 mL of 1 M NaOH at 85°C for 30 minutes. The residue was filtered. This alkali treatment was repeated thrice.¹⁴ The next step involved bleaching with 30% H_2O_2 for 20 minutes. Bleached cellulose precipitate was washed several times with distilled H_2O until reaching a neutral pH, filtered, dried in hot air oven.²⁶

Preparation of magnetite nanoparticles

Magnetite nanoparticles were synthesized by following (Singh et al. 2015) with slight modifications.²⁷ 27.0275 g of $\text{FeCl}_3 \cdot 6\text{H}_2\text{O}$, 9.94025 g of $\text{FeCl}_2 \cdot 4\text{H}_2\text{O}$ and 3.05 g of Urea was dissolved in 100 mL distilled water at 90°C for 2 hours. The mixture was cooled to room temperature. 1 M NaOH solution was added dropwise slowly with continuous stirring until pH

10. Black precipitate was washed with distilled water, centrifuged, dried in hot air oven.

Preparation of nanocomposite

DES was synthesized by mixing and heating choline chloride and D-Fructose in the molar ratio of 2:1 at 600 rpm and 80°C for 2 hours.²⁵ To 50 mL DES, 4 g of isolated cellulose and 1 g of magnetite nanoparticles were suspended and ultrasonicated for 15 mins, until the temperature reached 45°C. The change of colour from white to black indicated that the magnetite nanoparticles blended well with cellulose matrix. The mixture was cooled to room temperature, centrifuged, washed with distilled water and dried in hot air oven.

Characterization techniques

The compositional, structural, morphological and magnetic properties of the nanomaterials were characterized using Fourier transform infrared spectrophotometer, X-ray diffractometer, high-resolution transmission electron microscope and vibrational sample magnetometer. Briefly, Fourier transform infrared (FTIR) spectra were obtained using a Perkin Elmer Spectrum Two model with wavenumber range 4000 cm^{-1} to 400 cm^{-1} . X-ray diffraction (XRD) spectra were recorded on a D8 Advance Bruker X-ray diffractometer, in the range $2\theta = 10^\circ$ - 80° . An X-ray beam characteristic to Cu $K\alpha$ radiation was used ($\lambda = 0.15418$ nm). Geometrical evaluation (size and morphology), crystallinity were investigated using a Jeol/JEM 2100 high-resolution transmission electron microscope (HRTEM) operated at 200 kV with point resolution 0.23 nm. Selected area electron diffraction (SAED) for differentiating amorphous and crystalline nature was also performed. Magnetic parameters such as saturation magnetization, coercivity and retentivity were measured using a vibrational sample magnetometer (VSM, Model 7407, and Lakeshore, USA).

In vitro anticancer activity

The human ovarian cancer cell line (SKOV3) was purchased from the National Center for Cell Science (NCCS), Pune, India. MTT assay is a colorimetric method to measure cell viability worldwide. It is based on the reduction of a yellow tetrazolium salt [3-(4, 5-dimethylthiazol-2-yl)-2,5-diphenyltetrazolium bromide, or MTT] which helps to measure the cell viability. Viable cells contain NADPH dependent oxidoreductase enzymes which reduce the MTT reagent to formazan, a deep purple color insoluble crystalline salt. It is believed that dead cells do not reduce the MTT dye, whereas the live cells reduce the tetrazolium compound into the purple colored formazan through the mitochondrial enzyme. This formazan production is directly proportional to the viable cell count and inversely proportional to the degree of cytotoxicity. SKOV3 cells were grown in 96 well plate using DMEM supplemented with 10% FBS, 1% penicillin and streptomycin. Cells were treated with increasing concentration of nanomaterials 1.562, 3.125, 6.25, 12.5, 25, 50, 100 and 250 $\mu\text{g/mL}$ for 24 hours (except the untreated control). After the incubation period, the medium was discarded and 100 μL of MTT solution (5mg/mL) was added to each well and placed in 5% CO_2 incubator for 4 hours at 37°C. MTT solution was discarded and the formazan crystals were

dissolved in 50 μL of DMSO. Absorbances were read using Lark LIPR 9608 micro plate reader at 570 nm. Blank well contained only the medium. The experimental condition was replicated thrice and the IC_{50} values were obtained from an average of triplicate measurements.²⁸

Morphological changes in optical microscopy

To investigate the morphological changes, SKOV3 human ovarian cancer cells were seeded on 6 well tissue culture plates and treated with three different concentrations of cellulose, magnetite and cellulose-magnetite nanocomposite (250, 100 and 50 $\mu\text{g/mL}$) for 24 hours (except the untreated control) and observed under the optical microscope.²⁹

In vitro antitubercular activity

Mycobacterium tuberculosis H37Rv strain was obtained from the Microbial Type Culture Collection and Gene Bank (MTCC), Chandigarh, India. Luciferase reporter phage (LRP) assay is the most accurate test for screening antitubercular activity. It offers a simple procedure for drug sensitivity testing with relative accuracy, speed, ease, and low cost.³⁰ Luciferase Reporter Phages (LRPs) are phages harboring the luciferase gene, which produces visible light when expressed in the presence of an enzyme-substrate usually luciferin and cellular ATP. LRPs can infect, replicate and express their genome within live mycobacterial cells. When an LRP-infected clinical sample releases light after the addition of luciferin, the presence of viable *M. tuberculosis* is detected. When the sample is incubated with antibiotics followed by LRP infection, light emission is proportional to the resistance level. Luciferase activity can be monitored by quantifying the photons with a luminometer.³¹ The antitubercular activity of nanomaterials against *Mycobacterium tuberculosis* H37Rv was assessed using LRP assay.³² Briefly, about 350 μL of G7H9 broth supplemented with 10% albumin dextrose complex and 0.5% glycerol was taken in cryovials and added with 50 μL of each nanomaterial to get a final concentration of 200 $\mu\text{g/mL}$. 100 μL of *Mycobacterium tuberculosis* cell suspension was added to all the vials, DMSO (1%) served as solvent control. All the vials were incubated at 37°C for 72 hours. After incubation, 50 μL of high titer phage phAE129 and 40 μL of 0.1M CaCl_2 solutions were added to the test and control vials. All the vials were incubated at 37°C for 4 hours. After incubation, 100 μL of D-luciferin was added and the relative light unit (RLU) was measured immediately at 10 sec integration time in a luminometer (Lumat 9508, Berthold, Germany).

Statistical analysis

MTT assay was performed under triplicate condition; the results were expressed as Mean \pm Standard Deviation (SD). The calculations were made using Microsoft Excel 2013 software. Using the linear regression equation, IC_{50} values were calculated. Graphs were drawn using Origin software.

RESULTS AND DISCUSSION

FTIR analysis of cellulose, magnetite and cellulose-magnetite nanocomposite

Figure 1, 2 and 3 illustrated the FTIR spectra of cellulose, magnetite and cellulose-magnetite nanocomposite respectively.

Strong bands observed at 3411 cm^{-1} , 3372 cm^{-1} and 3368 cm^{-1} , are related to the O-H stretching vibrations of hydroxyl groups with strong inter and intra molecular H-bonding present in the samples.³³ As a result of nanocomposite formation, (Figure 3) cellulose chain scissions occur to various extents, leading to the presence of a different quantities of free O-H groups. This phenomenon can be esteemed from changes in broadening of hydroxyl peak, which may be due to the disruption of inter and intra molecular hydrogen bonding.³⁴ In figure 1 and 3, absorption bands at 2918 cm^{-1} and 2933 cm^{-1} denoted the C-H symmetric vibration of -CH- linkage, bands at 1429 cm^{-1} and 1479 cm^{-1} are due to C-H scissoring vibration of -CH- linkage,³¹ characteristic peaks of cellulose were evident at 1058 cm^{-1} and

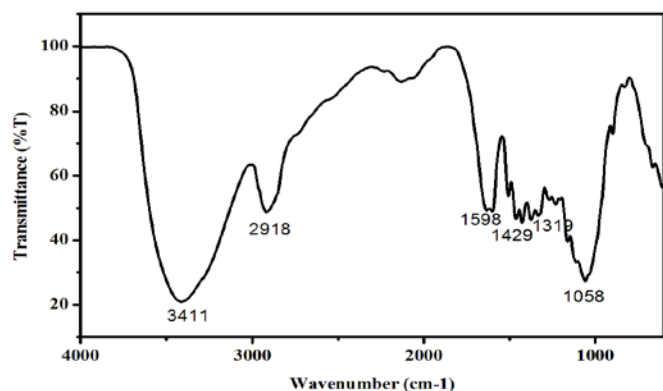


Figure 1. FTIR spectrum of isolated cellulose from fruit shells of *Limonia acidissima* (L.)

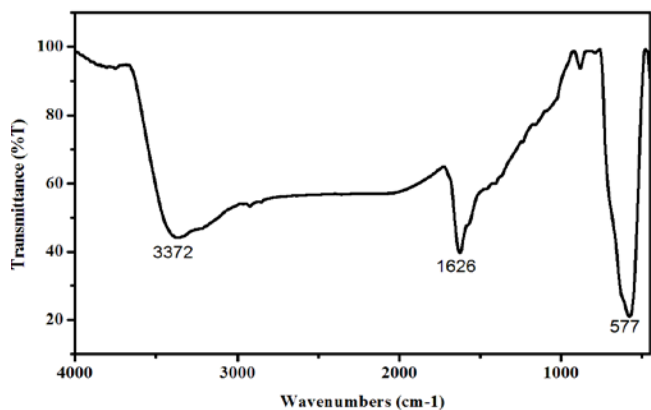


Figure 2. FTIR spectrum of magnetite nanoparticles

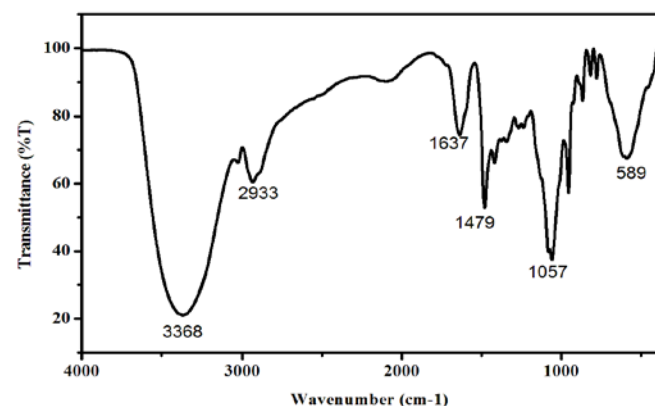


Figure 3. FTIR spectrum of cellulose-magnetite nanoparticles

1057 cm^{-1} owing to the C-O-C stretching vibrations of pyranose ring.³⁵ The less intense peak at 1319 cm^{-1} (Figure 1) indicated O-H in-plane bending vibration. Strong absorption at 1598 cm^{-1} (Figure 1) corresponded to C-C stretching vibration of the aliphatic component.³⁶ In Figures 2 and 3 vibrational absorptions at 1626 cm^{-1} and 1637 cm^{-1} have originated from the absorbed water.³⁷ Characteristic peaks at 577 cm^{-1} and 589 cm^{-1} denoted the Fe-O linkages.³⁸

XRD analysis of cellulose, magnetite and cellulose-magnetite nanocomposite

The XRD spectrum (Figure 4) presented the amorphous nature of isolated cellulose. Two peaks at $2\theta = 15.8^\circ$ and 22.5° corresponded to the two polymorphs of cellulose (I-alpha and I-beta).¹⁵ The characteristic crystalline planes (110), (200) and (004) corresponded to the typical cellulose-I structure.¹¹ The XRD spectrum (Figure 5) showed the crystalline planes of the cubic inverse spinel structure of magnetite (Fe_3O_4).³⁹ The XRD spectrum (Figure 6) indicated the cellulose-magnetite nanocomposite consisting of crystallographic planes (002), (220), (004) and (400). As expected, the XRD spectrum of cellulose-magnetite nanocomposite possessed characteristic peaks of both cellulose and magnetite which confirmed the integration of cellulose matrix onto the magnetite. The broadening of peaks proved the smaller size of the nanomaterials.⁴⁰

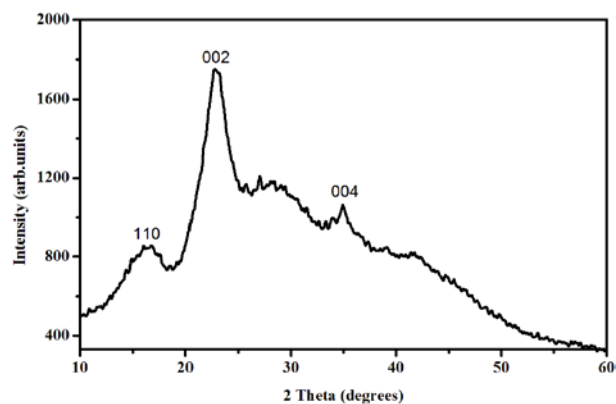


Figure 4. XRD pattern of isolated cellulose from fruit shells of *Limonia acidissima* (L.)

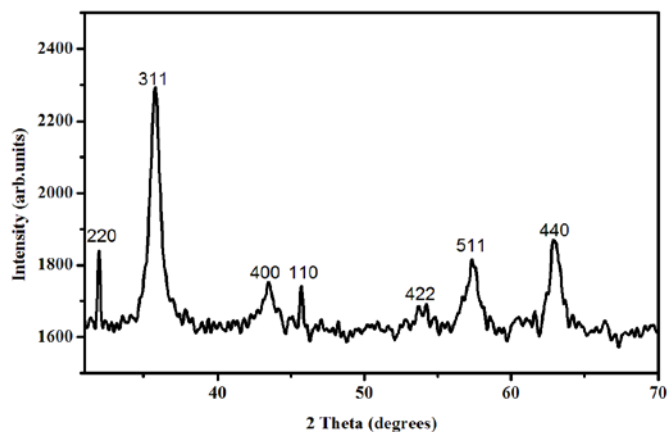


Figure 5. XRD pattern of magnetite nanoparticles

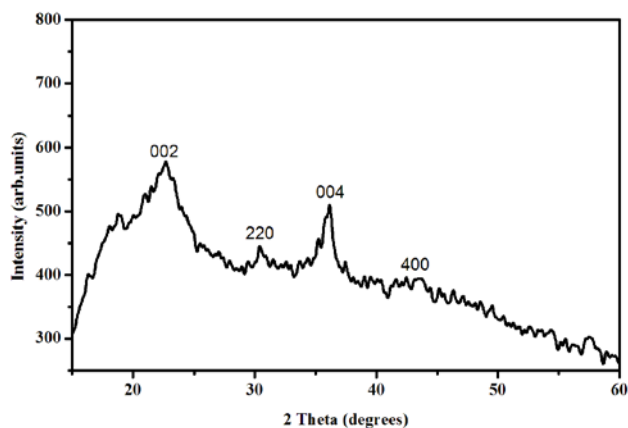


Figure 6. XRD pattern of cellulose-magnetite nanocomposite

The crystallite size was calculated using Scherrer's formula as mentioned in equation (1):

$$D = K\lambda / \beta \cos\Theta \quad (1)$$

Where, D is the crystallite size in nm, λ is the X-ray wavelength used ($\lambda = 0.15418$ nm), K is the shape factor ($K = 0.9$ for spherical particles), β is the full line width at the half-maximum elevation of the main intensity peak and Θ is the Bragg angle.

The calculated crystallite size for intense peaks (002), (311) and (002) of cellulose, magnetite nanoparticles and cellulose-magnetite nanocomposite were found to be 6.54 nm, 11.92 nm and 4.77 nm respectively.

TEM analysis of cellulose, magnetite and cellulose-magnetite nanocomposite

TEM analysis offers valuable evidence about the nanostructure, localization and dispersion of magnetite nanoparticles within the cellulose structure. TEM analysis was performed to study the presence of magnetite within the cellulose structure. Figure 7 (a-c) showed the TEM images of cellulose, magnetite nanoparticles and cellulose-magnetite nanocomposite respectively. The size of the materials depends on the synthesis protocol and experimental conditions.⁴¹ The nanomaterials were spherical with sizes ranging from 10 to 18 nm. Also, spherical shaped nanocellulose formation could be attributed to the self-assembly of short cellulose rods via interfacial hydrogen bonding.⁴² From the image (Figure 7c), the presence of magnetite onto the surface or within the cellulose is visualized. It is indicated that the nanocomposite prepared using DES is composed of individual well-distributed magnetite nanoparticles and cellulose onto and within the cellulose-magnetite nanocomposite, thus ascertaining the successful integration of cellulose and magnetite nanoparticles.

SAED analysis of cellulose, magnetite and cellulose-magnetite nanocomposite

SAED pattern was performed to analyze the crystallographic defects. Figure 8 (a-c) demonstrated the SAED patterns for cellulose, magnetite nanoparticles, cellulose-magnetite nanocomposite respectively. The d spacing was calculated using the electron diffraction equation as written in equation (2)

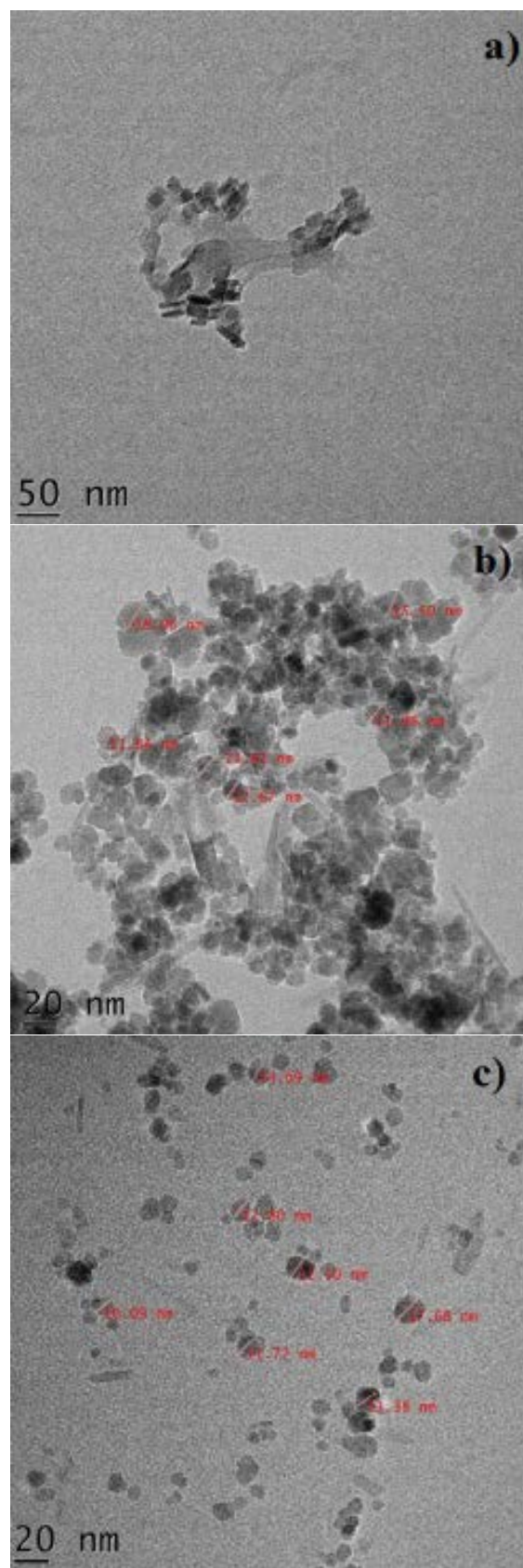


Figure 7. TEM images of **a)** isolated cellulose from fruit shells of *Limonia acidissima* (L.), **b)** magnetite nanoparticles and **c)** cellulose-magnetite nanocomposite

as follows:

$$L \lambda = d R \quad (2)$$

Where L is the distance between sample and electron micrograph, λ is the X-ray wavelength, and R is the radius of diffraction rings.⁴³ The d spacing obtained from XRD and SAED data are similar. Figure 8a showed a diffused rings with neither small spots nor concentric bright circles which confirmed that the isolated cellulose was purely amorphous. The concentric bright rings comprising of small spots (Figure 8b) confirmed that the magnetite nanoparticles were highly crystalline and those where of polycrystalline. The presence of characteristic concentric rings with tiny spots (Figure 8c) denoted the presence of planes corresponding to both cellulose and magnetite in the cellulose-magnetite nanocomposite.

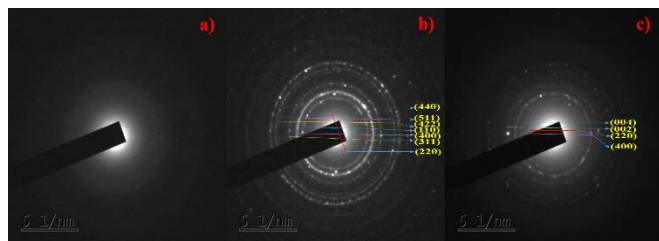


Figure 8. SAED patterns of **a)** isolated cellulose from fruit shells of *Limonia acidissima* (L.), **b)** magnetite nanoparticles and **c)** cellulose-magnetite nanocomposite

VSM analysis of magnetite and cellulose-magnetite nanocomposite

Magnetic parameters are tabulated in Table 1. It was observed that the value of retentivity and saturation magnetization for cellulose-magnetite nanocomposite was lower compared to that obtained for magnetite nanoparticles. Fabrication of cellulose into magnetite was responsible for the lower saturation magnetization and retentivity values for cellulose-magnetite nanocomposite. Magnetite nanoparticles are embedded in the cellulose matrix where each magnetite nanoparticle acts as a single magnetic domain with the least aggregation with a mild change in magnetization and a drastic decrease in the retentivity. Also, coercivity (H_{ci}) is lower (328.88 G and 332.21 G) for magnetite and cellulose-magnetite nanocomposite when compared to bulk magnetite (500-600 G), and coercivity does not decrease to zero due to the smaller particle size indicating super paramagnetic nature.³⁸ These results confirmed the higher loading and better distribution of cellulose in the nanocomposite. Because of the superparamagnetism, saturation magnetization (M_s) values for magnetite nanoparticles and cellulose-magnetite nanocomposite were 1.6013 emu/g and 0.2896 emu/g respectively which were much lower than that of the corresponding bulk magnetite 92emu/g.⁴⁴ Drastic reduction in saturation magnetization was attributed to factors such as smaller size of the nanomaterials, spherical shape, increased spin disorder at the surface, dipolar interaction between magnetite nanoparticles and a zero contribution from surface anisotropy, changes in A and B site population.^{45,46}

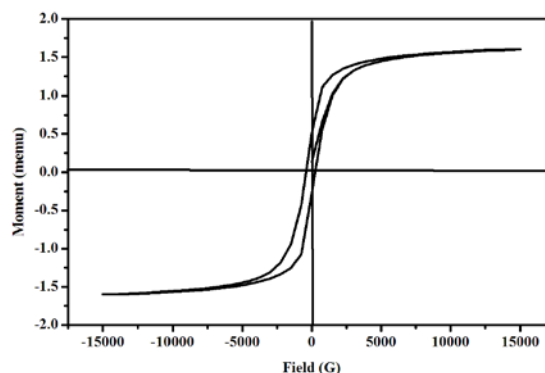


Figure 9. VSM hysteresis curve for magnetite nanoparticles

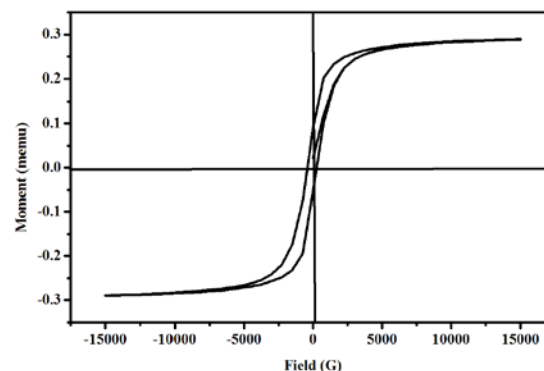


Figure 10. VSM hysteresis curve for cellulose-magnetite nanocomposite

Table 1: Magnetic properties of magnetite and cellulose-magnetite nanocomposite

Parameters	Magnetite nanoparticles	Cellulose-magnetite nanocomposite
Magnetization (M_s)	1.6013 emu	0.28961 emu
Coercivity (H_{ci})	328.88 G	332.21 G
Retentivity (M_r)	0.39637 emu	71.755 E ⁻³ emu
Squareness ratio (M_r/M_s)	0.2475 emu	0.2477 emu

Anticancer activity

Effect of nanomaterials on cell mortality

The percentage of live cells was calculated using equation,

$$\% \text{ of live cells} = (\text{Average optical density of treated cells} / \text{Average optical density of control cells}) \times 100\%$$

While the percentage of cell viability in the control group was assumed 100 %²⁸

The obtained IC_{50} values for cellulose, magnetite nanoparticles, and cellulose-magnetite nanocomposite were 20.65 $\mu\text{g/ml}$, 44.66 $\mu\text{g/ml}$, and 8.685 $\mu\text{g/ml}$ respectively. From Figure 11 and 12, it was clear that cellulose and magnetite

nanoparticles showed dose-dependent cytotoxic effect whereas (Figure 13) of cellulose-magnetite nanocomposite showed no dose-dependent toxicity. From Table 2, it was perceived that although both cellulose and magnetite individually possessed better cytotoxic properties, the cellulose-magnetite nanocomposite prepared using DES showed higher anticancer activity even at a lower concentrations. This confirmed the use of DES has an advantage in nanobiotechnology for better dispersion of nanomaterials and enhanced cytotoxic activities. Various criteria such as superparamagnetism, shape, smaller size, surface modification, the stability of nanomaterials play a vital role in drug delivery.⁴⁷ Superparamagnetic nanomaterials can be easily guided to a target site using the magnetic field. This advantage makes them versatile in targeted drug delivery with fewer side effects of chemotherapeutic drugs.⁴⁸ From VSM studies, it is concluded that the magnetite nanoparticles and cellulose-magnetite nanocomposite are superparamagnetic, thus enhancing the prospective use for targeted drug delivery without damaging healthy tissues. Among various morphologies, spherical shaped nanomaterials possesses significant advantages such as even surface coating and conjugation of ligands in surface functionalization, thereby more drug can be effectively loaded on the surface of nanoparticles for better drug release at the targeted site and thus exhibit effective cytotoxicity.⁴⁹ Total cell uptake in the drug delivery system was determined based on the size of nanomaterials. It was reported that particles with a size range 10-100 nm are effective as they exhibit longer circulation time in the body, elude the reticuloendothelial system in the body as well as penetrate through very small capillaries.⁴⁷ From TEM analysis, the size of nanomaterials in the range of 10-18 nm was found to be best suited for drug delivery. Surface modification and stability are other essential factors that can influence cytotoxicity. Uncoated magnetite tends to agglomerate and oxidize easily, thus surface coating makes them biocompatible with minimal toxicity to the human body.⁴⁹ In the present work the use of DES as a dispersant has improved the stability of nanocomposite. The natural components present in the DES has increased the cytotoxic activity as seen in (Figure 13)

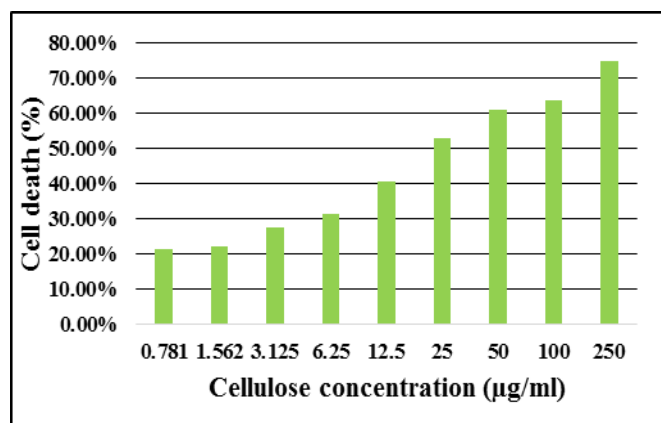


Figure 11. Plot showing % of cell death using cellulose isolated from *Limonia acidissima* (L.)

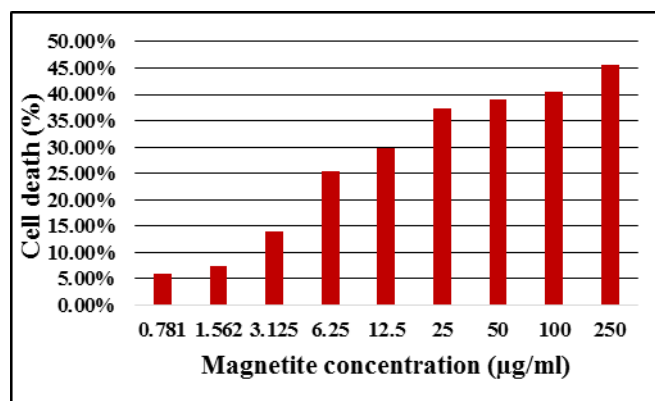


Figure 12. Plot showing % of cell death using magnetite nanoparticles

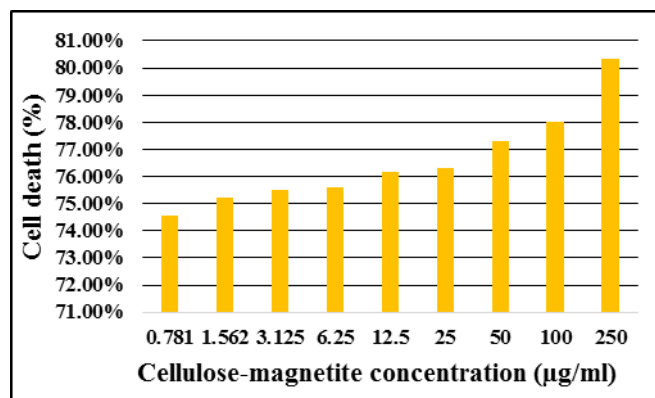


Figure 13. Plot showing % of cell death using cellulose-magnetite nanocomposite

Table 2: Anticancer activities of cellulose, magnetite nanoparticles and cellulose-magnetite nanocomposite expressed as Mean±Standard deviation.

Concentration (µg/ml)	% of cell death (Mean±Standard deviation)		
	Cellulose	Magnetite nanoparticles	Cellulose-magnetite nanocomposite
250	74.94±0.75	45.58±1.94	80.31±0.96
100	63.83±9.42	40.41±1.04	77.99±1.09
50	61.02±3.46	39.07±0.10	77.30±0.74
25	53.03±10.18	37.32±1.93	76.29±0.34
12.5	40.68±7.22	29.87±4.44	76.15±0.50
6.25	31.25±8.51	25.45±5.82	75.60±0.12
3.125	27.46±3.80	14.01±3.09	75.49±0.21
1.562	22.34±13.71	7.42±4.40	75.23±0.34
0.781	21.51±3.90	5.89±0.64	74.55±0.17

Effect of nanomaterials on morphological changes

Nanomaterials exposed to the SKOV3 human ovarian cancer cells led to characteristic apoptotic features such as a reduction in the cell number, shriveled cells, and lose contact with neighboring cells and detachment from tissue culture plate surface in comparison to the untreated control cells which retained its original morphology and were adhered to the surface of the tissue culture plates. These distinctive changes in cell morphology were attributed to the smaller size and large surface area of the nanomaterials which produces an increased level of reactive oxygen species (ROS).⁵⁰ Released ROS causes damage to nucleic acid and at high concentrations may lead to the breaking of hydrogen bonds in DNA structure, thereby resulting in cell death.⁵¹ Figure 14 revealed that the nanomaterials exhibited good activity over the cancer cells.

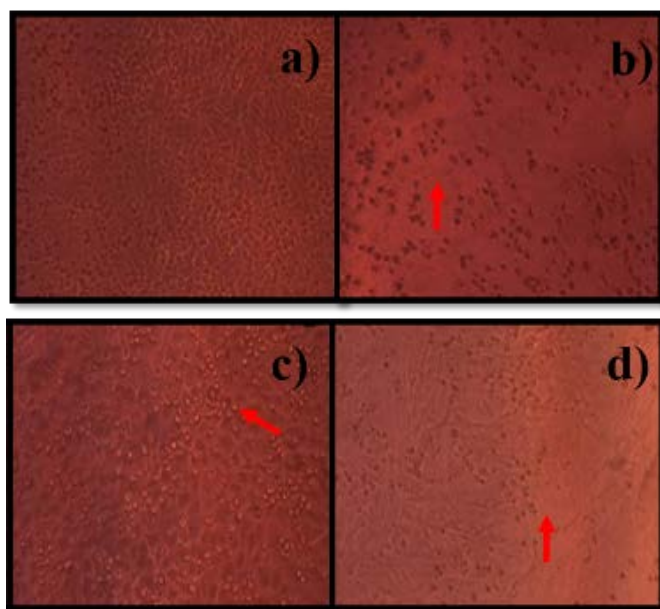


Figure 14. Morphological changes observed under optical microscope a) control SKOV3 human ovarian cancer cells, b)-d) SKOV3 human ovarian cancer cells treated with b) 50 µg/ml of isolated cellulose c) 50 µg/ml of magnetite nanoparticles d) 50 µg/ml of cellulose-magnetite nanocomposite for 24 hours (red arrow mark shows the shrunken cells)

Antitubercular activity

The antitubercular activity was tested against *Mycobacterium tuberculosis* H37Rv. The percentage of reduction in RLU was calculated using equation (10):

$$\% \text{ of reduction in RLU} = \frac{\text{Control RLU} - \text{Test RLU}}{\text{Control RLU}} \times 100\%$$

Antitubercular activities of cellulose, magnetite nanoparticles and cellulose-magnetite nanocomposite are shown in Figure 15. In LRP assay, with 200 µg/mL of cellulose, magnetite nanoparticles and cellulose-magnetite nanocomposite showed 18.67%, 33.85% and 51.95% RLU reduction respectively. Compounds/drugs with more than 50% of RLU reduction will be considered as having antitubercular activity.³² The as-synthesized cellulose-magnetite nanocomposite using DES has

shown antitubercular activity. This finding opens an avenue to use DES as a better dispersing agent for biomedical applications. It was reported a low concentration of 12.5 µg/mL of ZnO nanoparticles synthesized using lemon juice as a biofuel inhibited the growth of *Mycobacterium tuberculosis* H37Rv strain.⁵² The literature revealed that magnetic nanoparticles (MNPs) synthesized using co-precipitation method and coated with natural polymer chitosan and loaded with streptomycin to form a nano antibiotic could diagnose and treat tuberculosis infections.⁵³ With calcium carbonate as a template, inhalable superparamagnetic iron oxide nanoparticles were developed and used for pulmonary delivery of anti-TB drugs.⁵⁴

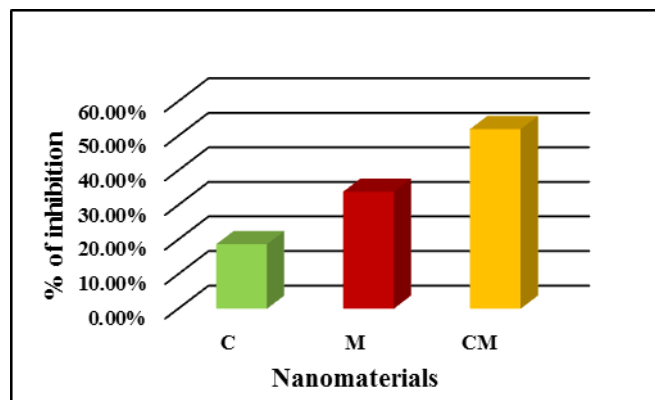


Figure 15. Bar graph depicting % of antitubercular activity at 200 µg/ml concentration of isolated cellulose (C), magnetite (M) and cellulose-magnetite (CM) nanocomposite

CONCLUSION

The anticancer and antitubercular activity of the DES mediated cellulose-magnetite nanocomposite was studied. VSM results of the synthesized magnetic nanomaterials exhibited no diamagnetism and were small enough to demonstrate superparamagnetic behavior. This superparamagnetic behavior of the produced nanomaterials can find use in magnetic hyperthermia treatment, targeted drug delivery and MRI imaging applications. TEM analysis confirmed that the nanomaterials are uniformly dispersed with a size of less than 20 nm. Due to their smaller size, these nanomaterials can find application in imaging tissues such as arteries, veins, capillaries and alveoli. The results obtained from MTT assay and LRP assay indicated that the cellulose-magnetite nanocomposite synthesized using choline chloride and D-Fructose based deep eutectic solvent (DES) has a strong effect on the SKOV3 human ovarian carcinoma cells and *Mycobacterium tuberculosis* H37Rv bacterial pathogen. The improved antitubercular and antitubercular activities of the cellulose-magnetite nanocomposite indicated that the use of DES composed of natural components had played a vital role in the enhancement of the observed biological activities. In conclusion, owing to its enriched physiochemical and biological properties as compared to pure magnetite and cellulose, the DES fabricated cellulose magnetite nanocomposite could be considered for next-level applications for in vivo anticancer and antitubercular studies.

CONFLICT OF INTEREST

The authors declare that there are no conflicts of interest with respect to the research, authorship, and/or publication of this article.

ACKNOWLEDGMENTS

The authors cordially thank DST FIST facility, CRIST lab, Stella Maris College, Chennai, IIT Madras, Sathyabama University, Chennai, St. Joseph's College, Trichy and STIC Cochin University, Kerala for rendering analytical facilities.

REFERENCES AND NOTES

- World Health Organization. WHO report on cancer: setting priorities, investing wisely and providing care for all. World Health Organization. 2020, 9789240001299-eng.pdf.
- D. Hanahan, R.A. Weinberg. The hallmarks of cancer. *Cell*. **2000**, 100, 57-70.
- Y. Lugani, S. Asthana, S. Labani. Ovarian carcinoma: an overview of current status. *Adv. Mod. Oncol. Res.* **2016**, 2, 261-270.
- C.N. Landen, M.J. Birrer, A.K. Sood. Early events in the pathogenesis of epithelial ovarian cancer. *J. Clin. Oncol.* **2008**, 26, 995-1005.
- D. Cameron, R. Bell. Optimizing treatment for patients with breast cancer. *Oncology*. **2004**, 31, 4-5.
- Global Tuberculosis Report. 2019. World Health Organization. 9789241565714-eng.pdf.
- F. Andrade, D. Rafael, M. Videira, D. Ferreora, A. Sosnik, B. Sarmiento. Nanotechnology and pulmonary delivery to overcome resistance in infectious diseases. *Advanc. Drug Deliv. Rev.* **2013**, 65, 1816-1827.
- P. Vijayvargia, R. Vijayvargia. A review on *Limonia acidissima* L.: multipotential medicinal plant. *Int. J. Pharm. Sci. Rev. Res.* **2014**, 36, 191-195.
- A.S. Sartape, A.M. Mandhare, V.V. Jadhav, P.D. Raut, M.A. Anuse, S.S. Kolekar. Removal of malachite green dye from aqueous solution with adsorption technique using *Limonia acidissima* (wood apple) shell as low cost adsorbent. *Arabian J. Chem.* **2017**, 10, S3229-S3238.
- C.H. Suresh, D.H.K. Reddy, Y. Harinath, B.R. Naik, K. Seshaiyah, A.V.R. Reddy. Development of wood apple shell (*Feronia acidissima*) powder biosorbent and its application for the removal of Cd (II) from aqueous solution. *The Sci. World J.* **2014**, 1-8.
- A. Kumar, Y.S. Negi, V. Choudhary, N.K. Bhardwaj. Characterization of cellulose nanocrystals produced by acid-hydrolysis from sugarcane bagasse as agro-waste. *J. Mater. Phys. Chem.* **2014**, 2, 1-8.
- R. Singanusong, W. Tochampa, T. Kongbangkerd, C. Sodchit. Extraction and properties of cellulose from banana peels. *J. Sci. Technol.* **2014**, 21, 201-213.
- P.L. Hariani, F. Riyanti, R.D. Asmara. Extraction of cellulose from kapok banana peel (*Musa parasidiaca* L.) for adsorption procion dye. *Molecul.* **2016**, 11, 135-142.
- M.S. Chagot, M. Chylinska, K. Gdula, A. Koziol, A. Zdunek. Isolation and characterization of cellulose from different fruit and vegetable pomaces. *Polymers.* **2017**, 9, 1-16.
- H. Tibolla, F.M. Pelissari, J.T. Martins, A.A. Vicente, F.C. Menegalli. Cellulose nanofibers produced from banana peel by chemical and mechanical treatments: characterization and cytotoxicity assessment. *J. Food. Hyd.* **2018**, 75, 192-201.
- S.B. Manjare, R.A. Chaudhari. Environment-friendly synthesis of palladium nanoparticles loaded on Zeolite Type-Y (Na-form) *Anacardium Occidentale* shell extract (Cashew nut shell extract), characterization and application in -C-C- coupling reaction. *Environ. Chem. Eng.* **2020**, 8, 104213.
- S.B. Manjare, R.A. Chaudhari. Palladium Nanoparticle-Bentonite Hybrid Using Leaves of *Syzygium aqueum* Plant from India: Design and Assessment in the Catalysis of -C-C- Coupling Reaction. *Chem. Africa.* **2020**, 3, 329-341.
- R. Rotaru, M. Savin, N. Tudorachi, C. Peptu, P. Samoila, L. Sacarescu, V. Harabagiu. Ferromagnetic iron oxide-cellulose nanocomposites prepared by ultrasonication. *Polymer Chem.* **2018**, 9, 860-868.
- A.P. Abbott, G. Capper, D.L. Davies, H.L. Munro, R.K. Rasheed, V. Tambyrajah. Preparation of novel moisture-stable, Lewis-acidic ionic liquids containing quaternary ammonium salts with functional side chains. *Chemical. Communications.* **2001**, 19, 2010-2011.
- K.R. Siongco, R.B. Leron, M.H. Li. Densities, refractive indices, and viscosities of N, N-diethylethanol ammonium chloride-glycerol or -ethylene glycol deep eutectic solvents and their aqueous solutions. *J. Chem. Thermodynamics.* **2013**, 65, 65-72.
- K.K. Kow, K. Sirat. Novel manganese (II)-based deep eutectic solvents: synthesis and physical properties analysis. *Chin. Chem. Lett.* **2015**, 1-4.
- A.A. Hamad, M. Hayyan, M.A.H. AlSaadi, M.A. Hashim. Potential applications of deep eutectic solvents in nanotechnology. *Chem. Engi. J.* **2015**, 1-57.
- C. Florindo, F.S. Oliveira, L.P.N. Rebelo, A.M. Fernandes, I.M. Marrucho. Insights into the synthesis and properties of deep eutectic solvents based on cholinium chloride and carboxylic acids. *ACS Sustain. Chem. Eng.* **2014**, 2, 2416-2425.
- S.H. Zeisel, K.A. Costa. Choline: an essential nutrient for public health. *Nutritional Reviews.* **2009**, 67, 615-623.
- A. Hayyan, F.S. Mjalli, I.M. AlNashef, T. Al-Wahaibi, Y.M. Al-Wahaibi, M.A. Hashim. Fruit sugar-based deep eutectic solvents and their physical properties. *Thermochimica. Acta.* **2012**, 541, 70-75.
- T. Prakhongpan, A. Nitithamyong, P. Luanpituksa. Extraction and application of dietary fiber and cellulose from pineapple cores. *J. Food. Sci.* **2002**, 67, 1308-1313.
- N. Singh, D. Mondal, M. Sharma, R.V. Devkar, S. Dubey, K. Prasad. Sustainable processing and synthesis of non-toxic and antibacterial magnetic nanocomposite from spider silk in neoteric solvents. *ACS Sustainable Chem. Eng.* **2015**, 1-21.
- T. Mosmann. Rapid colorimetric assay for cellular survival: application to proliferation and cytotoxicity assays. *J. Immunol. Methods.* **1983**, 65, 55-63.
- P. Moongkarndi, N. Kosem, S. Kaslungka, O. Luanratana, N. Pongpan, N. Neungton. Antiproliferation, antioxidation and induction of apoptosis by *Garcinia mangostana* (mangosteen) on SKBR3 human breast cancer cell line. *J. Ethnopharmacol.* **2004**, 90, 161-166.
- G. Sivaramakrishnan, B. Subramanyam, C. Ponnuraja, V. Kumar. Luciferase reporter phage phAE85 for rapid detection of rifampicin resistance in clinical isolates of *Mycobacterium tuberculosis*. *Asian Pacific J. of Trop. Med.* **2013**, 728-731.
- P.F. Riska, W.R. Jacobs, Jr., B.R. Bloom, J. McKittrick, J. Chan. Specific identification of *Mycobacterium tuberculosis* with the luciferase reporter mycobacteriophage: use of p-nitro-alpha-acetylamino-beta-hydroxy propiophenone. *J. Clin. Microbiol.* **1997**, 35, 3225-3231.
- R. Manikkam, S. Ponnuswamy, J. Joseph, V. Kumar. Antitubercular activity of the pigment from forest soil *Streptomyces* sp SFA5. *Bangladesh. J. Pharmacol.* **2016**, 11, 138-140.
- K.L. Wang, N. Jiang, B.B. He, D.X. Kang. Regiocontrol synthesis cellulose-graft-polycaprolactone copolymer (2,3-di-O-PCL-cellulose) by a new route. *EXPRESS Polymer Letters.* **2017**, 11, 991-1002.
- S. Elanthikkal, U. Gopalakrishnanpanicker, S. Varghese, J.T. Guthrie. Cellulose microfibrils produced from banana plant wastes: Isolation and characterization. *Carbohydrate Polymers.* **2010**, 80, 852-859.
- B. Deepa, E. Abraham, N. Cordeiro, M. Mozetic, A.P. Mathew, K. Oksman, M. Faria, S. Thomas, L.A. Pothan. Utilization of various lignocellulosic biomass for the production of nanocellulose: A comparative study. *Cellulose.* **2015**, 22, 1075-1090.
- X. Colom, F. Carrillo, F. Nogues, P. Garriga. Structural analysis of photodegraded wood by means of FTIR spectroscopy. *Polymer Degradation and Stability.* **2003**, 80, 543-549.
- S. Naduparambath, T.V. Jinita, V. Shaniba, M.P. Sreejith, K.B. Aparna, E. Purushothaman. Isolation and characterisation of cellulose

- nanocrystals from sago seed shells. *Carbohydrate Polymers*. **2018**, 180, 13-20.
38. A. Kaushik, P.R. Solanki, A.A. Ansari, G. Sumana, S. Ahmad, B.D. Malhotra. Iron oxide-chitosan nanobiocomposite for urea sensor. *Sens. Actuators, B: Chemical*. **2009**, 138, 572.
 39. F. Chen, S.L. Xie, J. Zhang, R. Liu. Synthesis of spherical Fe₃O₄ magnetic nanoparticles by co-precipitation in choline chloride/urea deep eutectic solvent. *Mater. Lett.* **2013**, 112, 177-179.
 40. R. Yogamalar, R. Srinivasan, A. Vinu, K. Ariga, A.C. Bose. X-ray peak broadening analysis in ZnO nanoparticles. *Solid State Communi.* **2009**, 149, 1919-1923.
 41. Martinez-Sanz, L.A. Rubio, J.M. Lagaron. Optimization of the nanofabrication by acid hydrolysis of bacterial cellulose nanowhiskers. *Carbohydrate Polymers*. **2011**, 85, 228-236.
 42. Berg O van den, J.R. Capadona, C. Weder. Preparation of homogeneous dispersions of tunicate cellulose whiskers in organic solvents. *Biomacromolecules*. **2007**, 8, 1353-1357.
 43. W.B. Wu, Y. Jing, M.R. Gong, X.F. Zhou, H.Q. Dai. Preparation and properties of magnetic cellulose fiber composites. *BioResources*. **2011**, 6, 3396-3409.
 44. R.M. Cornell, U. Schwertmann. The iron oxides: structure, properties, reactions, occurrences and uses. **2004**, (2nd edn), Wiley VCH Weinheim, Germany.
 45. M.P. Morales, M. Andres-Verges, S. Veintemillas-Verdaguer, M.I. Montero, C.J. Serna. Structural effects on the magnetic properties of gamma-Fe₂O₃ nanoparticles. *J. Magn. Magn. Mater.* **1999**, 203, 146-148.
 46. F. Bodker, S. Morup, S. Linderth. Surface effects in metallic iron nanoparticles. *Phys. Rev. Lett.* **1994**, 72, 282-285.
 47. Y.P. Yew, K. Shamel, M. Miyake, N.B.B.A. Khairudin, S.E.B. Mohamad, T. Naiki, K.X. Lee. Green biosynthesis of superparamagnetic magnetite Fe₃O₄ nanoparticles and biomedical applications in targeted anticancer drug delivery system: a review. *Arabian J. Chem.* **2020**, 13, 2287-2308.
 48. B. Chertok, B.A. Moffat, A.E. David, F. Yu, C. Bergemann, B.D. Ross, V.C. Yang. Iron oxide nanoparticles as a drug delivery vehicle for MRI monitored magnetic targeting of brain tumors. *Biomaterials*. **2008**, 29, 487-496.
 49. A. Ali, H.M.Z. Zafar, I. ul Haq, A.R. Phull, J.S. Ali, A. Hussain. Synthesis, characterization, application and challenges of iron oxide nanoparticles. *Nanotechnol. Sci. Appl.* **2016**, 9, 49-67.
 50. P.V. Kumar, A.J. Ahamed, M. Karthikeyan. Synthesis and characterization of NiO nanoparticles by chemical as well as green routes and their comparisons with respect to cytotoxic effect and toxicity studies in microbial and MCF-7 cancer cell models. *SN Appl. Sci.* **2019**, 1, 1083.
 51. S.J.H. Soenen, E. Illyes, D. Vercautern, K. Braeckmans, Z. Majer, S.C. De Smedt. The role of nanoparticle concentration-dependent induction of cellular stress in the internalization of non-toxic cationic magnetoliposomes. *Biomaterials*. **2009**, 30, 6803-6813.
 52. P.G. Krishna, P.P. Ananthaswamy, P. Trivedi, V. Chaturvedi, N.B. Mutta, A. Sannaiah, A. Erra, T. Yadavalli. Antitubercular activity of ZnO nanoparticles prepared by solution combustion synthesis using lemon juice as bio-fuel. *Mater. Sci. and Engin: C*. **2017**, 75, 1026-1033.
 53. M.E.E. Zowalaty, S.H.H.A. Ali, M.I. Hussein, B.M. Geilich, T.J. Webster, M.Z. Hussein. The ability of streptomycin-loaded chitosan-coated magnetic nanocomposites to possess antimicrobial and antituberculosis activities. *Intern. J. Nanomed.* **2015**, 10, 3269-3274.
 54. M.S. Miranda, M.T. Rodrigues, R.M.A. Domingues et.al. Development of inhalable superparamagnetic iron oxide nanoparticles (SPIONs) in microparticulate system for antituberculosis drug delivery. *Adv. Healthcare Mater.* **2018**, 1800124, 1-12.